Copolymers of 2-(9*H*-Carbazol-9-yl)ethyl 2-Methylacrylate and 4-[5-(4-*tert*-Butylphenyl)-1,3,4-oxadiazol-2-yl]phenyl 2-Methylacrylate: Correlating Hole Drift Mobility and Electronic Structure Calculations with Electroluminescence

David D. Evanoff, Jr.,[†] Justin R. Lawrence,[‡] Christopher F. Huebner, J. Michael Houchins, Brian J. Stevenson, Alexandra L. Foguth, Joseph B. Carroll,[§] and Stephen H. Foulger*

Center for Optical Materials Science and Engineering Technologies, School of Materials Science and Engineering, Clemson University, Clemson, South Carolina 29634-0971

ABSTRACT Methacrylate monomers functionalized with pendant carbazole and oxadiazole moieties were copolymerized into random copolymers with varying carbazole/oxadiazole ratios. Specifically, the monomers of 2-(9*H*-carbazol-9-yl)ethyl 2-methylacrylate (CE) and 4-[5-(4-*tert*-butylphenyl)-1,3,4-oxadiazol-2-yl]phenyl 2-methylacrylate (tBPOP) were copolymerized in various ratios, and the inherent hole drift mobilities were assessed through time-of-flight techniques. At a field strength of 345 kV/cm, the homopolymer PCE exhibited a hole mobility of 5.9×10^{-7} cm^2/V · s, which was approximately twice the value of the technologically important poly(9-vinylcarbazole), which exhibited a value of 2.8×10^{-7} cm^2/V · s. The range of hole mobilities in the copolymers varied from 2.4×10^{-8} cm^2/V · s for copolymers containing 50 mol % of the carbazole-containing monomer residue to 3.0×10^{-7} cm^2/V · s for copolymers that incorporated 88 mol % of the residue. Density functional theory (B3LYP/6-21G*) and optical absorption derived highest occupied molecular orbital (HOMO) and lowest unoccupied molecular orbital (LUMO) energies of CE were −5.39 and −1.94 eV, respectively, while the corresponding oxadiazole monomer (tBPOP) had a HOMO energy of −5.99 eV and a LUMO energy of −2.23 eV. The mean luminous efficiency of coumarin 6 doped single-layer devices constructed from the poly(CE-*co*-tBPOP) copolymers indicated a relatively flat efficiency of ca. 0.25 cd/A over a wide carbazole mole fraction content of 0.30−0.70.

KEYWORDS: organic light emitting diode • electroluminescence • density functional theory

1. INTRODUCTION

Technologies involved in the creation of artificial light have seen a steady increase in their efficiency, with current incandescent systems typically exhibiting a luminous efficacy of 10−18 lm/W and current semiconductor devices that exploit electroluminescence (EL) routinely surpassing 80−90 lm/W (1). Organic light-emitting devices (OLEDs) couple the prospect of printable device fabrication with luminous efficacies greater than 100 lm/W. A typical OLED consists of, in the following order, a hole-injecting electrode, a hole-transport layer, an emissive layer, an electron-transport layer, and an electron-injecting electrode. Electrons and holes that are injected into the device from the electrodes recombine in the light-emitting layer, creating an excited state that decays to the ground state by emitting a photon. The various layers are typically less than 100 nm thick, and frequently the charge-transport and emission functions are combined into a single layer.

In order to construct an OLED with optimal efficiency and device lifetime, holes and electrons must be injected into the device at a rate to achieve similar densities of the two carriers. In a recent effort from our laboratory, methacrylate copolymers functionalized with pendant carbazole and oxadiazole moieties (cf. Figure 1) were synthesized and exploited in single-layer devices (2). Specifically, the monomers of 2-(9*H*-carbazol-9-yl)ethyl 2-methylacrylate (CE) and 4-[5-(4-*tert*-butylphenyl)-1,3,4-oxadiazol-2-yl]phenyl 2-methylacrylate (tBPOP) were synthesized and copolymerized in various CE/tBPOP ratios to explore the photo- and electroluminescent properties of the copolymers, which were referred to as poly(CE$_x$-*co*-tBPOP$_{1-x}$), where x represents the carbazole content in mol %. These polymeric thin films are highly resistive, low-mobility solids, and the drift mobilities of the materials are difficult to measure using general methods. There is a dearth of information on these poly(CE-*co*-tBPOP) copolymers for use in OLEDs, and the current effort focuses on establishing the inherent hole-mobility

* To whom correspondence should be addressed. E-mail: foulger@clemson.edu.
Received for review December 18, 2008 and accepted March 4, 2009

[†] Current address: Department of Chemistry & Physics, Western Carolina University, Cullowhee, NC 28723.

[‡] Current address: Centre for Advanced Functional Materials & Devices, University of Wales, Cardiff, U.K.

[§] Current address: Cabot Corp., Billerica, MA 01821.

DOI: 10.1021/am800248g

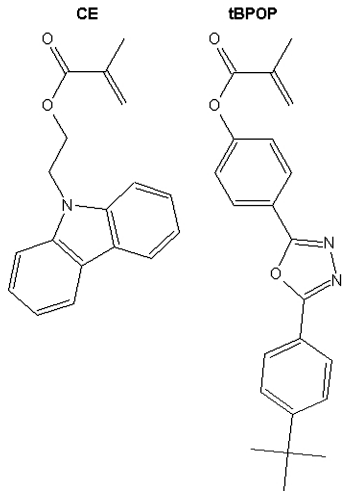

FIGURE 1. Methacrylate monomers with pendant carbazole [2-(9*H*-carbazol-9-yl)ethyl 2-methylacrylate (CE)] and oxadiazole [4-[5-(4-*tert*-butylphenyl)-1,3,4-oxadiazol-2-yl]phenyl 2-methylacrylate (tBPOP)] moieties utilized to form the corresponding random copolymer.

characteristics through time-of-flight techniques of these copolymers as a function of the CE/tBPOP ratio.

2. EXPERIMENTAL SECTION

Materials. 2-(4-*tert*-Butylphenyl)-5-(4-biphenylyl)-1,3,4-oxadiazole (tBu-PBD), zinc (99.995%, 100 mesh), 3-(2-benzothiazolyl)-7-(diethylamino)coumarin (coumarin 6), and calcium (99.99%) were purchased from Aldrich and used as received. Poly(9-vinylcarbazole) (PVK; M_w = 1.1 million) was also purchased from Aldrich and precipitated three times into methanol prior to use to remove any contaminants. 2-Propanol (70%), acetone, hydrochloric acid (37%), chlorobenzene (ACS grade), and potassium hydroxide were purchased from Fisher Scientific. Chlorobenzene was dried over molecular sieves prior to use. 3,4-Poly(ethylenedioxythiophene)/poly(styrenesulfonate) (PEDOT/PSS) was purchased from H. C. Stark and filtered through a 0.45-μm filter before use. Aluminum (99.99%) was purchased from Kurt J. Lesker Co. Unpolished ITO-coated float glass (8−12 $\Omega \cdot$ cm) was purchased from Delta Technologies. The syntheses of the poly(CE-*co*-tBPOP) copolymers have been presented elsewhere (2).

Characterization Methods. Absorption spectra of the polymers [diluted to 10 μg/mL in tetrahydrofuran (THF)] were taken using a Perkin-Elmer Lambda 850 spectrophotometer. Photoluminescence (PL) spectra were collected using a Jobin-Yvon Fluorolog 3-222 Tau spectrometer. All device fabrication and performance testing was completed in an MBraun Unilab glovebox under an argon atmosphere (O_2 and $H_2O \leq 1$ ppm). Polymer films were spun cast onto substrates using a Specialty Coating Systems G3-P8 spin coater. Cathode deposition was done in a Denton 502 vacuum evaporation chamber. The polymer film thickness was measured using a Tencor Instruments Alpha-step 200 profilometer. Current−voltage characteristics of the devices were measured using a Keithley 228A current−voltage source and a Keithley 2001 digital multimeter. Luminance measurements were made using a Konica-Minolta LS-110 luminance meter. For the time-of-flight study, a Photon Technology International GL 3300 nitrogen laser, a Keithley 6517A electrometer, and an Agilent Technologies 200 MHz digital storage oscilloscope were employed. The film capacitance was measured using a QuadTech 7600 RLC meter. EL spectra were obtained in an inert atmosphere using a Jobin Yvon MicroHR spectrometer coupled to a Jobin Yvon Synapse CCD detector.

Time-of-Flight Analysis. ITO anodes with a surface area of 3.6 cm^2 were patterned on 6.5 cm^2 substrates using HCl (with zinc powder) to etch unwanted ITO. The patterned substrates were ultrasonicated in acetone and then isopropyl alcohol, which was followed by an air plasma treatment to remove any surface contamination. Copolymer solutions (typically 250 mg/mL) were prepared in an argon atmosphere using dry, degassed chlorobenzene. Films were spun cast at a speed that would yield 5−15-μm-thick films as measured by contact profilometry. An aluminum cathode was deposited (base pressure ca. 2×10^{-6} Torr) onto the substrates at 3−5 Å/s to a final thickness of 150 nm. The samples were biased such that ITO was at a positive potential. An oscilloscope, triggered by a laser, measured the voltage drop across a variable resistor (set to 25−30 kΩ), which was connected to an aluminum electrode. A 1-ns pulse of 337-nm radiation was used to excite the copolymers. Neutral density filters were employed to keep the energy per laser pulse between 3 and 15 μJ.

Fabrication and Characterization of OLEDs. ITO anodes with a surface area of 0.4 cm^2 were patterned on 1.6 cm^2 substrates using HCl (with zinc powder) to etch unwanted ITO. The patterned substrates were ultrasonicated in acetone and then isopropyl alcohol, which was followed by an air plasma treatment to remove any surface contamination. To aid in hole injection for polymer/small-molecule blend devices, a 50−70-nm film of PEDOT/PSS was spun cast onto the substrates and annealed for 25 min at 85 °C on a hot plate, while copolymer-based devices did not incorporate PEDOT/PSS. Copolymer solutions were prepared in an argon atmosphere using dry, degassed chlorobenzene. Copolymer-based devices had films that were spun cast at a speed that would yield 100-nm-thick films as measured by contact profilometry, typically 3000 rpm from a 40 mg/mL solution, while polymer/small-molecule blend devices were made from films spun cast at 2000 rpm from 20−40 mg/mL solutions. All polymer solutions used for devices contained 0.3 wt % coumarin 6. Cathodes were deposited (base pressure ca. 2×10^{-6} Torr) onto the substrates through a steel shadow mask that resulted in two 2.5-mm metal strips running perpendicular to the ITO anode. The cathode consisted of a 30-nm layer of calcium deposited at 1−2 Å/s and a 100-nm layer of aluminum deposited at 3−5 Å/s.

Devices were positioned in the glovebox such that the emitting surface was parallel to the collection optics of the luminance meter, which was outside the glovebox; the typical distance between an OLED and the luminance meter was ca. 30 cm. Current−voltage−luminance characteristics were recorded automatically through the use of a simple BASIC program. Voltage was ramped in 1 V increments per second, while current and luminance values were simultaneously recorded.

3. RESULTS AND DISCUSSION

3.1. Charge-Transport Properties. The hole mobility of PVK, PCE, and the poly(CE-*co*-tBPOP) copolymers were measured through time-of-flight experiments. In the current context, time-of-flight refers to the time required for a hole to propagate across a thin film under an applied electric field. The experimental setup utilized for these measurements was adopted from a previous effort (3). A number of experimental parameters were controlled to ensure reliable mobility values, including the energy of the incident light, the time constant of the resistance × capacitance (RC) circuit, the removal of the excess charge from the circuit, and the absorption of the polymer film. Typically, a neutral density filter with an outside diameter of 3 cm was used to limit the energy of the nanosecond laser pulse to less than 15 μJ (4). The RC time constant for the test circuit was controlled by

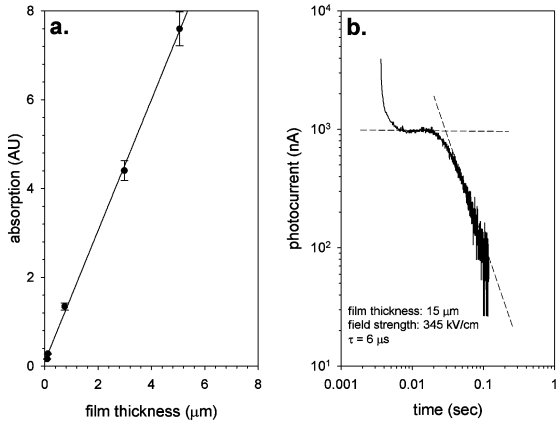

FIGURE 2. (a) Absorption of PVK with film thickness and (b) transient characteristics of a typical photogenerated current in a PVK film. Measurements were taken at 23 °C.

measuring the capacitance of the polymer films with an inductor capacitor resistor (LCR) meter using a standard four-probe configuration and selecting a resistance value from an inline decade resistor. The resistance value was chosen to both minimize the time constant of the circuit, to ensure that the time required to transport the holes across the polymer film was much longer than the response of the testing circuit, and maximize the voltage drop across the sample, to assist in making reliable voltage measurements. For our experimental configuration, typical transit times were one to tens of milliseconds, depending on the film thickness and the applied field. Utilizing a resistor value of 25−30 kΩ resulted in a time constant that was 2−3 orders of magnitude shorter than the transit time of the holes. To ensure that any trapped charge in the film was drained to the ground, the films were left in the dark for 20 min under bias between experimental runs.

A critical parameter in any time-of-flight experiment is to ensure that the "sheet" of excitons created by the laser pulse is much thinner than the total thickness of the polymer film being studied. The relationship between the film thickness of PVK and absorption at 337 nm is presented in Figure 2a. At least 95% of the incident radiation is absorbed in the first 800 nm of the PVK film; all polymer films employed in this effort were 6−10 times thicker than this value.

Figure 2b presents the temporal change in the photogenerated current after a 15-μm-thick PVK film, biased at a field strength of 345 kV/cm, was pulsed with a 337-nm laser; hole-transit times were found by inspecting the intersection of the tangent lines of the curve (4, 5). From Figure 2b, the hole mobility is 2.8×10^{-7} cm^2/V · s for PVK at the above field strength, a value similar to published data (3, 5−8).

Figure 3 presents hole-mobility values for PVK over a range of field strengths. In this system, mobility is a thermally activated process where the activation energy decreases with an increasing field strength. Hole and electron mobilities in PVK exhibit an electric field and temperature dependence that can be described by an empirically derived relationship of the form

$$\mu(E, T) = \mu_0 \exp\left(-\frac{\varepsilon_0}{kT_{\text{eff}}}\right) \exp\left(\frac{\beta E^{1/2}}{kT_{\text{eff}}}\right) \quad (1)$$

where μ_0 is a function of the film composition, β is a constant coefficient, k is Boltzmann's constant, ε_0 is the activation energy, E is the electric field magnitude, and T_{eff} is the effective temperature (3).

Figure 3 also presents the mobility values for PCE and indicates that this homopolymer exhibits hole mobilities that are twice as large as those of PVK at similar field strengths; these measurements were repeated several times and yielded similar results. In such low-mobility solids, it is expected that hopping conduction dominates and is characterized by incoherent jumps of carriers between isolated molecular sites (9). The underlying reason for the enhanced hole mobility in PCE relative to PVK is speculated to stem from a diminished level of excimer formation in PCE. Previous studies on the hole drift mobility in PVK employed a model system to establish that a decreasing hole mobility correlated to an increasing excimer fluorescence yield of the model compounds (10). It was concluded that charge trapping at the excimer-forming sites results in a drop in the charge-carrier mobility.

Previous studies on the PL characteristics of the homopolymers PVK and PCE, at similar molecular weights and concentrations, indicate that the spectra are significantly different between the two polymers (cf. Figure 4), with the spectrum of PCE being similar to its monomer emission in the spectral position, shape, and width (2). Conversely, the spectrum of PVK exhibits significant red tailing, indicative of excimer emission stemming from the sterically confined carbazole units along the chain adopting an intramolecular parallel overlap arrangement (11). Excimer emission in these carbazole-based polymers requires excimer-forming geometries to exist prior to being excited or to form during the monomeric excited-state lifetime, and the close proximity

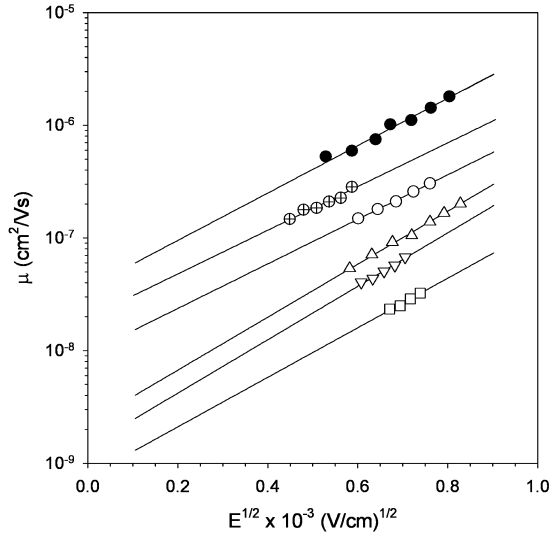

FIGURE 3. Hole mobility as a function of the applied electric field for PVK (⊕), PCE (●), poly(CE_{88}-*co*-t$BPOP_{12}$) (○), poly(CE_{78}-*co*-t$BPOP_{22}$) (△), poly(CE_{67}-*co*-t$BPOP_{33}$) (▽), and poly(CE_{50}-*co*-t$BPOP_{50}$) (□). Measurements were taken at 23 °C.

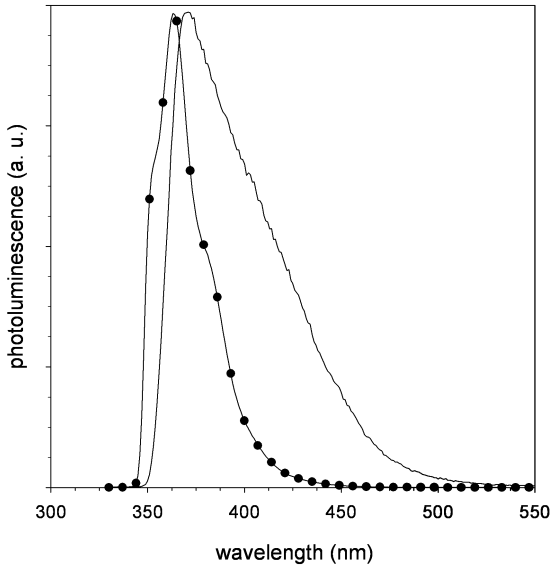

FIGURE 4. PL spectra of PVK (—) and PCE (—●—) in THF. Solutions were at a concentration of 1.0 mg/mL; the excitation wavelength was 315 nm.

of the chromophores can result in the formation of an excimer between excited-state and spatially adjacent ground-state chromophores (12). The long linkage from the polymer backbone to the carbazole ring in PCE, relative to PVK, offers an enhanced flexibility to the chromophore and diminishes the probability of parallel ring overlap for excimer formation. The mutual chromophore separation, orientation, and mobility are vital in controlling the photophysics of polymers with pendant π-conjugated rings (13, 14).

The hole mobilities of the poly(CE-*co*-tBPOP) copolymers were also measured at a range of electric field strengths and are presented in Figure 3. As the carbazole concentration in the copolymers is reduced, the overall magnitude of the hole mobilities in a copolymer diminishes. This is not an unexpected result because the reduction of carbazoles in the bulk polymer film would necessarily result in a larger distance between potential hopping sites for the holes. In the continuous-time random-walk model, often invoked for describing charge-carrier transport in an amorphous medium (5), the hopping rate W for charge transport at a set temperature exhibits an exponential dependence in the distance between potential sites, i.e., $W \propto e^{-r/r_0}$, where r is the distance between hopping sites and r_0 characterizes the range of interaction responsible for hopping. The poly(CE-*co*-tBPOP) copolymers have a random sequencing of carbazole and oxadiazole monomer residues in the polymer backbone (2), and the replacement of some portion of the carbazole moieties with oxadiazole moieties would statistically raise the value of r between hopping sites.

3.2. EL. EL (cf. Figure 5a) of the copolymers when in an ITO/polymer/Ca/Al single-layer device appeared to mimic their corresponding PL responses, with the addition of peaks at 550 and 605 nm that can be attributed to electromer emission (15, 16). PL spectra of the copolymer films exhibited a main emission peak at 394 ± 2 nm, with shoulders at ca. 350 and 370 nm. The shoulders can be largely attributed to the monomer-like emission of the carbazole-containing

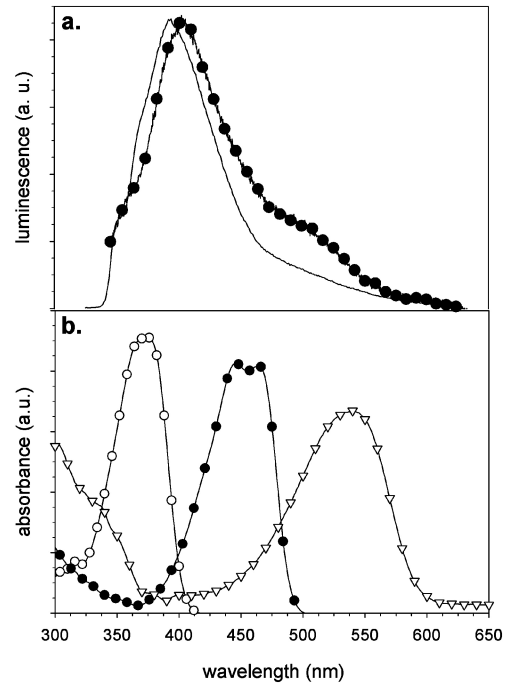

FIGURE 5. (a) PL spectrum (—) of poly(CE_{72}-*co*-$tBPOP_{28}$) in a chlorobenzene solution (1.0 mg/mL; the excitation energy was at a wavelength of 315 nm) and the corresponding EL spectrum (●) when in an ITO/polymer/Ca/Al single-layer device. (b) Absorption spectra of dyes routinely utilized in OLEDs: coumarin 1 (○), coumarin 6 (●), and nile red (▽).

monomer residue, though the oxadiazole contribution is evident in the 370-nm shoulder with copolymers of decreasing carbazole content (2). The main 394-nm emission peak is unique to the copolymers, is not present in the homopolymer films, and is suggestive of exciplex formation, through either intra- or interchain interactions. The appearance of this new band in the copolymer film emission spectra as compared to the solution spectra is not accompanied by new bands in the copolymer PL excitation or absorption spectra, and the absorption spectra of copolymer films overlay the solution absorption spectra. These characteristics suggest that the species responsible for the emission at 394 nm is not directly accessed optically, an indication of an excited-state interaction rather than a simple ground-state aggregation of the chromophores (17, 18).

For optimal performance of a single-layer donor/acceptor-based OLED, the energy associated with an emission in the host must be transferred to a fluorescent or phosphorescent dye through Förster or Dexter energy transfer; i.e., the emission of the polymer should overlap the absorption of the dye used in the device. In Figure 5b, the absorbance of three common fluorescent dyes typically used in PVK/tBu-PBD systems—coumarin 1, coumarin 6, and nile red—is presented. The overlap in absorption of the dyes with the EL emission of the poly(CE_{72}-*co*-$tBPOP_{28}$) device (cf. Figure 5a) is relatively good, with the green (coumarin 6) and red (nile red) dyes exhibiting a significant level of overlap. Similar to PVK/tBu-PBD systems, coumarin 6 provides the highest degree of overlap and was the dye used for this study. For all devices studied, the polymer solution used for spin-casting contained 0.3 wt % dye (19).

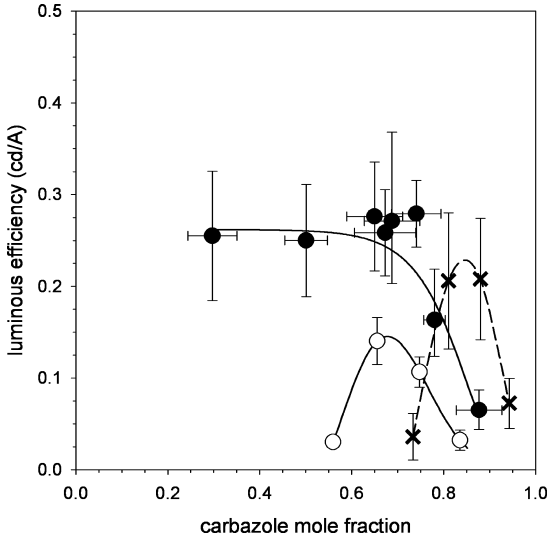

FIGURE 6. Mean luminous efficiency with a carbazole-to-oxadiazole ratio of coumarin 6 doped single-layer devices composed of PVK/tBu-PBD (×) blends, PCE/tBu-PBD blends (○), and poly(CE-*co*-tBPOP) copolymers (●). Curves are guides for the eye. Error bars represent the standard deviation of the mean based on 6−8 pixels.

In order to baseline the performance of the copolymers in single-layer OLEDs, devices were constructed with either PVK or PCE, which were physically blended with tBu-PBD and an EL dye. These devices were fabricated according to well-established literature techniques and included spin-casting films from solutions containing polymer, tBu-PBD, and coumarin 6 onto PEDOT/PSS-coated ITO substrates and, subsequently, evaporating calcium and aluminum cathodes onto the assembly (20).

In Figure 6, the mean luminous efficiencies of PCE/tBu-PBD and PVK/tBu-PBD devices are presented as a function of the carbazole-to-oxadiazole ratio (21). The overall efficiency of the PVK-based device is ca. 0.20 cd/A, which is greater than 0.14 cd/A seen in the PCE-based devices, though there is significant overlap of the mean values within the standard deviation. Nonetheless, the maximum efficiency for the PCE system occurs at a significantly lower carbazole-to-oxadiazole ratio relative to the PVK-based systems. While the highest luminance efficiency of the PVK devices occurs at a carbazole mole fraction of 0.82, a value similar to what has been reported in previous efforts (19, 22), the PCE devices are most efficient at a carbazole mole fraction of 0.67. This latter result seems plausible in light of the higher hole mobility of PCE relative to PVK (cf. Figure 3) because the PCE/tBu-PBD systems would require a greater concentration of tBu-PBD to balance the charge flow.

Figure 7 presents the current−voltage−luminance characteristics of a typical device fabricated with each of the poly(CE-*co*-tBPOP) copolymers. The current and luminance turn-on voltages for each copolymer composition, determined by the intersection of the tangent lines of the two linear portions of the curve, are quite similar across the copolymer compositions. While the carbazole-to-oxadiazole ratio is certainly important to achieving a balanced charge flow, it is quite surprising to see the wide range of carbazole-to-oxadiazole ratios that still give equivalent luminance and current turn-on voltages.

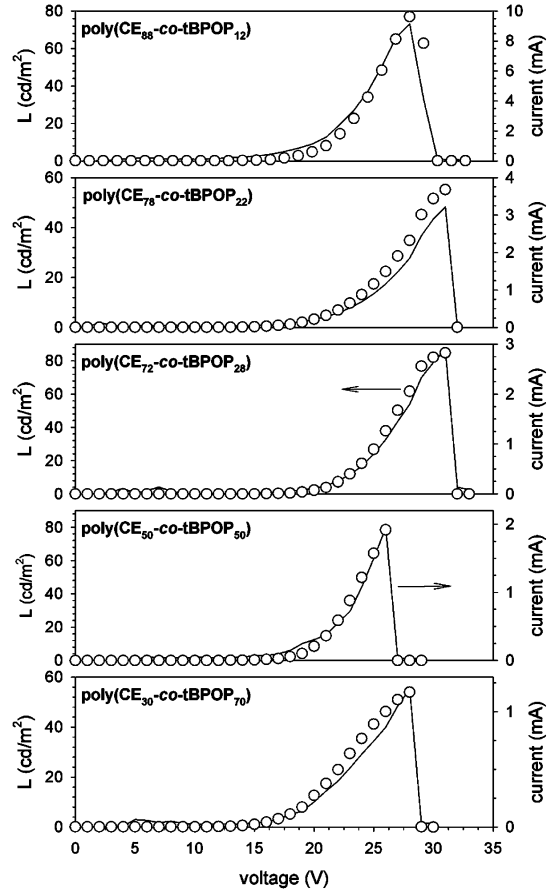

FIGURE 7. Luminosity (○) and current (—) at various applied voltages for ITO/(polymer and coumarin 6)/Ca/Al single-layer devices with various poly(CE-*co*-tBPOP) polymers.

Table 1. Current−Voltage−Luminance Characteristics of Poly(CE-*co*-tBPOP) Copolymers[a]

copolymer	voltage (V)	current (mA)	luminance (cd/m^2)
poly(CE_{88}-*co*-$tBPOP_{12}$)	24 ± 1	7.6 ± 2.2	59 ± 13
poly(CE_{78}-*co*-$tBPOP_{22}$)	28 ± 1	2.4 ± 0.5	48 ± 10
poly(CE_{72}-*co*-$tBPOP_{28}$)	32 ± 1	1.8 ± 0.9	57 ± 20
poly(CE_{50}-*co*-$tBPOP_{50}$)	27 ± 1	2.2 ± 0.6	67 ± 16
poly(CE_{30}-*co*-$tBPOP_{70}$)	29 ± 1	1.4 ± 0.4	45 ± 13

[a] Voltage and current (mean ± standard deviation) based on 6−8 pixels and measured at the observed maximum luminance.

Table 1 presents the current−voltage−luminance characteristics of a number of devices constructed from copolymers with varying CE/tBPOP ratios. The mean and standard deviation of the voltage and current, based on a sampling of 6−8 pixels, were obtained at the maximum observed luminance of the device. On the basis of the relatively high turn-on voltages and low luminosities, the performance of the devices is not optimized relative to single-layer devices (23, 24) or comparable PVK-based single-layer devices, although, interestingly, the devices exhibit a minimal dependence on the copolymer composition.

The lack of compositional dependence in the performance for the copolymers is apparent in Figure 6, which

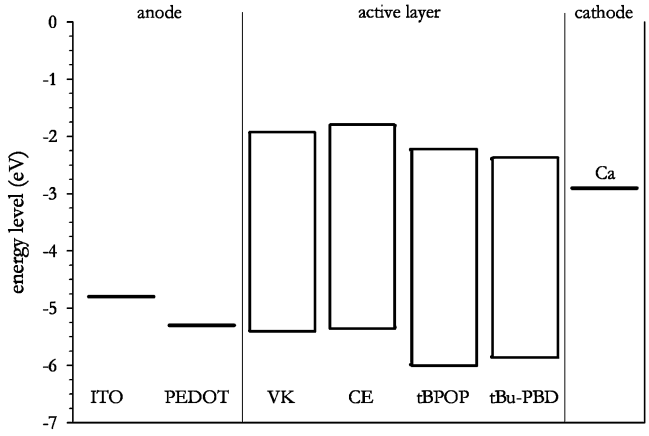

FIGURE 8. Schematic depicting a comparison of the energy levels of different materials utilized in a single-layer OLED. Active layer values were taken from Table 2.

presents the luminous efficiency of coumarin 6 doped single-layer devices constructed from the poly(CE-*co*-tBPOP) copolymers compared to PCE/tBu-PBD physical blend devices. The copolymer-based devices exhibit a relatively flat efficiency of ca. 0.25 cd/A over a wide carbazole mole fraction content of 0.30−0.70, dropping to lower efficiencies with higher carbazole contents. The corresponding PCE/tBu-PBD blend devices exhibit a peaked luminous efficiency profile with a maximum of ca. 0.14 cd/A at a carbazole mole fraction content of 0.67. In fact, the onset point for decreasing efficiency in the copolymer devices appears to coincide with the maximum efficiency of the blend devices.

3.3. Electronic Structure Calculations. It is well-known that the energy profile of an OLED (cf. Figure 8) is a critical design parameter in the successful operation of the device. The interfaces between electrodes and the materials in the active layer are central to the performance of the device because the mismatch between the Fermi energy of the electrodes and the highest occupied molecular orbital (HOMO) and lowest unoccupied molecular orbital (LUMO) controls the charge injection into the device. The work function (ϕ_w) of the electrodes, relative to the copolymer, determines the respective barriers to charge injection and the corresponding turn-on voltage. In these types of systems, the anode is ITO (ϕ_w = 4.7−4.8 eV) or PEDOT/PSS (ϕ_w = 5.05−5.65 eV) (25) coated on ITO, while the cathode is typically a low work function metal, such as calcium (ϕ_w = 2.9 eV) or aluminum (ϕ_w = 4.3 eV). The relatively high operating voltages observed in the current poly(CE-*co*-tBPOP) system may be due to the energy-level mismatch between the copolymers and the calcium cathode of the device. To assess this possibility, the electronic properties of the monomers were calculated by using density functional theory (DFT) with the 6-21G* basis set. The DFT approach utilized the three-parameter hybrid-exchange functional of Beckel and the Lee−Yang−Parr correlation functional (B3LYP) (26).

Table 2 presents the DFT-derived HOMO−LUMO energies (relative to a vacuum) for the materials of interest. Because of computational restrictions, only the monomers were studied. This is not a limitation in comparing the calculated systems to the experimental results because charge transport occurs in these species through hopping from one moiety (oxadiazole and carbazole) to the next and its attachment to a polymerizable vinyl or methacrylate group does not significantly alter its intrinsic electronic characteristics (9); quantum-mechanical (QM) calculations on vinylcarbazole (VK) as a monomer and as a trimer did not indicate significant differences in the electronic characteristics.

Table 2. QM Electronic Structure Calculations and Experimentally Observed Energies of Charge-Transport Systems (All Energies Are Expressed in eV)

		B3LYP/6-21G*			
	experimental ΔE_{op}[a]	HOMO	LUMO	ΔE	$LUMO_{op}$[b]
VK	3.44	5.39	0.76	4.63	1.94
CE	3.52	5.33	1.31	4.02	1.81
tBu-PBD	3.46	5.85	1.66	4.19	2.39
tBPOP	3.76	5.99	1.66	4.33	2.23

[a] Electronic absorption band edge. [b] Value based on the difference of the calculated HOMO energy and the energy at the experimentally observed electronic absorption band edge (27).

On the basis of a simple criterion of matching energetic profiles, Table 2 indicates that the carbazole-containing monomer (CE) is an adequate replacement for VK because its DFT-derived HOMO energy is only 0.06 eV higher, which is within the thermal energy contribution at a typical device operating temperature. With DFT calculations, there exists a linear correlation relationship between the calculated HOMO/LUMO energies and the experimentally observed ionization potential (IP) and electron affinity, allowing calculated HOMO and LUMO energies to be used semiquantitatively to estimate the IP and electron affinity (28, 29). Nonetheless, the agreement between calculated LUMO energies and experimental electron affinities is often quite poor. Therefore, Table 2 also presents LUMO energies based on the difference of DFT-derived HOMO values and the energy at the experimentally observed optical electronic absorption band edge. Employing this procedure results in the LUMO values of tBu-PBD and tBPOP differing by 0.16 eV. Nonetheless, there is a significant barrier to electron injection because of the difference between the electron affinity of tBPOP (2.23 eV) and the work function of calcium (2.9 eV); this may account for the relatively high turn-on voltages of the poly(CE-*co*-tBPOP) devices (cf. Table 1). This mismatch will also effect the luminance efficiency because, for a given copolymer, a maximum recombination probability is obtained when the two carrier concentrations are of equal level. Optimization of the electrode through its replacement with another low-work-function metal or the use of a tailored bilayer electrode (30) may improve the performance of the current system.

4. CONCLUSIONS

The monomers of CE and tBPOP were copolymerized in various carbazole-to-oxadiazole ratios, and the inherent hole

drift mobilities were assessed through time-of-flight techniques. At a field strength of 345 kV/cm, the homopolymer PCE exhibited a hole mobility of 5.9×10^{-7} $cm^2/V \cdot s$, which was approximately twice the 2.8×10^{-7} $cm^2/V \cdot s$ value exhibited by the technologically important polymer PVK. The range of hole mobilities in the copolymers varied from 2.4×10^{-8} $cm^2/V \cdot s$ for copolymers containing 50 mol % of the carbazole-containing monomer residues to 3.0×10^{-7} $cm^2/V \cdot s$ for copolymers that incorporated 88 mol % of the residue. The mean luminous efficiency of coumarin 6 doped single-layer devices constructed from the poly(CE-*co*-tBPOP) copolymers indicated a relatively flat efficiency of ca. 0.25 cd/A over a wide carbazole mole fraction content of 0.30—0.70. The lack of compositional sensitivity in the copolymer devices is a benefit to OLED designers, where the ultimate performance of the device is decoupled from the thermomechancial characteristics of the copolymers, such as the glass transition or solubility parameter, allowing designers a wider operational window for fabricating devices.

Acknowledgment. The authors thank DARPA (Grant N66001-04-1-8933), the National Science Foundation through a CAREER award (Grant DMR-0236692 to S.H.F.), the Gregg—Graniteville Foundation, and the State of South Carolina for financial support.

REFERENCES AND NOTES

(1) http://www.netl.doe.gov/ssl/, U.S. Department of Energy, Energy Efficiency and Renewable Energy.
(2) Evanoff, D. D., Jr.; Carroll, J. B.; Roeder, R. D.; Hunt, Z. J.; Lawrence, J. R.; Foulger, S. H. *J. Polym. Sci., Part A: Polym. Chem.* **2008**, *46*, 7882–7897.
(3) Gill, W. D. *J. Appl. Phys.* **1972**, *43*, 5033–5040.
(4) Bos, F. C.; Burland, D. M. *Phys. Rev. Lett.* **1987**, *58*, 152–155.
(5) Bos, F. C.; Guion, T.; Burland, D. M. *Phys. Rev. B* **1989**, *39*, 12633–12641.
(6) Grazulevicius, J. V.; Strohriegl, P.; Pielichowski, J.; Pielichowski, K. *Prog. Polym. Sci.* **2003**, *28*, 1297–1353.
(7) Pai, D. M.; Yanus, J. F.; Stolka, M. *J. Phys. Chem.* **1984**, *88*, 4714–4717.
(8) Pai, D. M. *J. Chem. Phys.* **1970**, *52*, 2285.
(9) Arkhipov, V. I.; Emelianova, E. V.; Tak, Y. H.; Bassler, H. *J. Appl. Phys.* **1998**, *84*, 848–856.
(10) Yokoyama, M.; Akiyama, K.; Yamamori, N.; Mikawa, H.; Kusabayashi, S. *Polym. J.* **1985**, *17*, 545–548.
(11) Johnson, G. E. *J. Phys. Chem.* **1974**, *78*, 1512–1521.
(12) Birks, J. B. *Nature (London)* **1967**, *214*, 1187–1190.
(13) Itoh, Y.; Yasue, T.; Gouki, M.; Hachimori, A. *Polymer* **1996**, *37*, 5433–5437.
(14) Nakahira, T.; Ishizuka, S.; Iwabuchi, S.; Kojima, K. *Macromolecules* **1983**, *16*, 297–302.
(15) Kalinowski, J.; Giro, G.; Cocchi, M.; Fattori, V.; Di Marco, P. *Appl. Phys. Lett.* **2000**, *76*, 2352–2354.
(16) Lee, Y. Z.; Chen, X. W.; Chen, M. C.; Chen, S. A.; Hsu, J. H.; Fann, W. *Appl. Phys. Lett.* **2001**, *79*, 308–310.
(17) Blatchford, J. W.; Jessen, S. W.; Lin, L. B.; Gustafson, T. L.; Fu, D. K.; Wang, H. L.; Swager, T. M.; MacDiarmid, A. G.; Epstein, A. J. *Phys. Rev. B* **1996**, *54*, 9180–9189.
(18) De Lucia, F. C.; Gustafson, T. L.; Wang, D.; Epstein, A. J. *Phys. Rev. B* **2002**, *65*, XXX.
(19) Luszczynska, B.; Dobruchowska, E.; Glowacki, I.; Ulanski, J.; Jaiser, F.; Yang, X. H.; Neher, D.; Danel, A. *J. Appl. Phys.* **2006**, *99*, 4.
(20) Johnson, G. E.; McGrane, K. M.; Stolka, M. *Pure Appl. Chem.* **1995**, *67*, 175–182.
(21) Forrest, S. R.; Bradley, D. D. C.; Thompson, M. E. *Adv. Mater.* **2003**, *15*, 1043–1048.
(22) Yang, X. H.; Neher, D.; Hertel, D.; Daubler, T. K. *Adv. Mater.* **2004**, *16*, 161+.
(23) Tsai, M. L.; Liu, C. Y.; Hsu, M. A.; Chow, T. J. *Appl. Phys. Lett.* **2003**, *82*, 550–552.
(24) Chuen, C. H.; Tao, Y. T. *Appl. Phys. Lett.* **2002**, *81*, 4499–4501.
(25) Koch, N.; Vollmer, A.; Elschner, A. *Appl. Phys. Lett.* **2007**, *90*, 3.
(26) Barrio, L.; Catalan, J.; de Paz, J. L. G. *Int. J. Quantum Chem.* **2003**, *91*, 432–437.
(27) Du, B.; Wang, L.; Wu, H. B.; Yang, W.; Zhang, Y.; Liu, R. S.; Sun, M. L.; Peng, J. B.; Cao, Y. *Chem.—Eur. J.* **2007**, *13*, 7432–7442.
(28) Zhan, C. G.; Nichols, J. A.; Dixon, D. A. *J. Phys. Chem. A* **2003**, *107*, 4184–4195.
(29) Chong, D. P.; Gritsenko, O. V.; Baerends, E. J. *J. Chem. Phys.* **2002**, *116*, 1760–1772.
(30) Hung, L. S.; Tang, C. W.; Mason, M. G. *Appl. Phys. Lett.* **1997**, *70*, 152–154.

AM800248G